PROTEINS
STRUCTURE ■ FUNCTION ■ BIOINFORMATICS

Combining crystallography and molecular dynamics: The case of *Schistosoma mansoni* phospholipid glutathione peroxidase

Daniela Dimastrogiovanni,[1] Massimiliano Anselmi,[2] Adriana Erica Miele,[1] Giovanna Boumis,[1] Linn Petersson,[1] Francesco Angelucci,[1] Alfredo Di Nola,[2] Maurizio Brunori,[1] and Andrea Bellelli[1]*

[1] Dipartimento di Scienze Biochimiche A. Rossi Fanelli and Istituto Pasteur, Fondazione Cenci Bolognetti, "Sapienza" University of Rome, Rome, Italy

[2] Dipartimento di Chimica, "Sapienza" University of Rome, Rome, Italy

ABSTRACT

Oxidative stress is a widespread challenge for living organisms, and especially so for parasitic ones, given the fact that their hosts can produce reactive oxygen species (ROS) as a mechanism of defense. Thus, long lived parasites, such as the flatworm Schistosomes, have evolved refined enzymatic systems capable of detoxifying ROS. Among these, glutathione peroxidases (Gpx) are a family of sulfur or selenium-dependent isozymes sharing the ability to reduce peroxides using the reducing equivalents provided by glutathione or possibly small proteins such as thioredoxin. As for other frontline antioxidant enzymatic systems, Gpxs are localized in the tegument of the Schistosomes, the outermost defense layer. In this article, we present the first crystal structure at 1.0 and 1.7 Å resolution of two recombinant SmGpxs, carrying the active site mutations Sec43Cys and Sec43Ser, respectively. The structures confirm that this enzyme belongs to the monomeric class 4 (phospholipid hydroperoxide) Gpx. In the case of the Sec to Cys mutant, the catalytic Cys residue is oxidized to sulfonic acid. By combining static crystallography with molecular dynamics simulations, we obtained insight into the substrate binding sites and the conformational changes relevant to catalysis, proposing a role for the unusual reactivity of the catalytic residue.

Proteins 2009; 00:000–000.

Key words: atomic resolution crystal structure; ROS detoxification pathway; schistosomiasis; lipid GSH peroxidase; molecular dynamics simulations.

INTRODUCTION

Aerobic organisms have evolved various nonenzymatic and enzymatic systems to detoxify reactive oxygen species (ROS), thereby limiting the adverse effects of these damaging compounds. Among the enzymes involved in the cellular response to oxidative stress are several glutathione-dependent enzymes, like glutaredoxins (Grx), glutathione peroxidases (Gpx), thioredoxin reductases (TR), and glutathione reductases (GR).

Gpxs represent a family of enzymes with complex evolutionary relationships and characterized by various activities, reducing partners and cellular localizations.[1] Some Gpxs are selenoproteins[2] using glutathione (GSH) to catalyze the reduction of H_2O_2 and organic hydroperoxides, but recently several nonselenium Gpx with cellular activities different from their canonical antioxidant role have been identified.[3]

Selenium-containing Gpxs have a functionally relevant residue of Selenium Cysteine (Sec), encoded by a TGA codon,[4,5] in the active site. Sec is required for full catalytic efficiency, as shown by point mutation or *in vivo* Se depletion[6]; and the Sec to Cys mutant Gpxs studied so far present a variable degree of functional impairment with respect to their wild type counterparts.[7] The presence of Sec has aroused interest on Gpx, due to the *in vivo* relevance of selenoproteins[8]; however, the known difficulties in heterologous expression of native selenoenzymes represent a practical problem.[9]

Although the classification of Gpxs is complex and has been repeatedly revised, it seems that seleno Gpxs may still be classified into four

Abbreviations: βME, beta-mercaptoethanol; DTT, dithiothreitol; EDTA, 2-[2-(Bis(carboxymethyl)amino)ethyl-(carboxymethyl)amino]acetic acid; Gpx, glutathione peroxidases; Grx, glutaredoxin; GSH, glutathione; GST, glutathione-S-transferase; PMSF, phenylmethanesulfonyl fluoride; ROS, reactive oxygen species; Sm, *Schistosoma mansoni*; Trx, thioredoxin; TCEP, tris(2-carboxyethyl)phosphine; U43C SmGpx, Sec43Cys mutant SmGpx; U43S SmGpx, Sec43Ser mutant SmGpx.

Grant sponsors: "Sapienza" University of Rome (Progetto Università 2006 e Ateneo Federato), MIUR Italy (FIRB/Biologia strutturale and FIRB/Proteomica); Grant numbers: 2003-RBLA03B3KC_004, 2007-prot RBRN07BMCT; Grant sponsor: European Community—Research Infrastructure Action (FP6 "Structuring the European Research Area" Programme); Grant number: R II 3-CT-2004-506008.
*Correspondence to: Andrea Bellelli, Dipartimento di Scienze Biochimiche, "Sapienza" University of Rome, piazzale Aldo Moro 5, Rome 00185, Italy. E-mail: andrea.bellelli@uniroma1.it
Received 9 February 2009; Revised 4 June 2009; Accepted 24 June 2009
Published online in Wiley InterScience (www.interscience.wiley.com).
DOI: 10.1002/prot.22536

major groups: Gpx1 (cellular or cytosolic[10]), Gpx2 (gastrointestinal[11]), Gpx3 (plasmatic or extracellular, which use Trx instead of GSH as reducing substrate[12]), Gpx4 (phospholipid hydroperoxide Gpx[13]). An additional isozyme, closely related to class 3 Gpxs, has been detected in the olfactory epithelium and assigned to class 6, whose members are either selenium (in humans) or sulfur based (in rodents).[1] Only a few Gpxs have been structurally characterized, including the enzymes from bovine erythrocytes and from human plasma (both homotetramers, M.W. = 84 KDa, with one Sec and one GSH binding site per subunit). Bovine and human enzymes, though classified as cytosolic (Gpx1) and extracellular (Gpx3), display a very similar organization of residues in the catalytic site, with two highly conserved amino acids: Gln and Trp.[10,12] These two residues seem to be crucial for enzymatic activity, being localized at hydrogen bonding distance from Sec; recent results suggest that also the conserved Asn residue closer to Trp may play a role during catalysis.[14]

The same pattern of catalytic residues is present also in class 4 Gpxs. Gpx4 have been found in different organisms from mammals to parasites,[13] to plants[15] and seem to be involved in many cellular processes, from regulation of apoptosis to protection of biological membranes from oxidative stress.[16–19] Indeed the latter function discriminates class 4 from all other family members. Few functional studies of Gpx4 are available, and the structure of two Sec mutants of human phospholipid-hydroperoxide Gpx (HsGpx4) (i.e., Sec to Cys[20] and Sec to Gly[21] mutants) has been solved, confirming the monomeric state and the conserved catalytic residues.

We have focused our work on a Gpx4 from *Schistosoma mansoni*, an important human parasite causative agent of a neglected disease responsible for about 280,000 deaths per year in tropical and subtropical areas.[22] Since vaccines, though actively studied, are of modest efficacy, the best available defense against the disease is chemotherapy with Praziquantel,[23] because other drugs are poorly used given that toxicity and/or lower efficacy. The search of new drugs and new molecular targets is therefore imperative, and is made possible by the extensive information available on the parasite's genome.

As Schistosomes are parasites living in the blood stream, they need protection against ROS released by the human host in response to invasion.[24] The worms possess several antioxidant enzymes,[25] which cooperate in a complex redox pathway to finally detoxify H_2O_2 and organic hydroperoxides, protecting the parasite and contributing to its survival. Thus, a structural elucidation of the parasite antioxidant enzymes may prove useful to identify new possible pharmacological targets.[26–28]

A *S. mansoni* gene encoding for a 19.4 KDa Se-containing Gpx, with a 53% amino acid sequence identity to human HsGpx4, has been identified.[29–31] Functional studies confirmed the existence of a specific Gpx in the worms, sharing molecular weight, substrate specificity and catalytic efficiency with mammalian HsGpx4. These results were confirmed by measurements of SmGpx activity toward H_2O_2 and cumene hydroperoxide in various fractions of worm extracts from different developmental stages.[32] Recently, Sayed et al.[28] identified one additional Gpx gene (SmGpx2) with 55 and 48% identity with SmGpx and human HsGpx4, respectively, but less than 36% identity to other classes of human Gpxs. This confirmed that both SmGpx proteins belong exclusively to the Gpx4 class.[28]

In this article, we present the structure of a Sec43Cys mutant of *S. mansoni* glutathione peroxidase (U43C SmGpx) at atomic resolution (1.0 Å), together with molecular dynamic simulations describing the geometry and motions of the functionally relevant protein clefts. Superposition with the other structurally characterized Gpx4 (human HsGpx4) helped exploring a peculiarity of U43C SmGpx, whose active site Cys, at least under some experimental conditions, undergoes spontaneous oxidation to sulfonic acid, not reported for the same Sec/Cys mutant of HsGpx4. By combining this comparison with molecular dynamics simulation and factors affecting the redox state of Cys residues,[33] we concluded that the *in vitro* reactivity of this residue may reflect special redox properties of SmGpx *in vivo*, possibly responsible for its peculiarities relative to other known Gpxs. To test whether the oxidation of Cys43 to the bulkier sulfonic acid altered the structure of SmGpx, we resorted to a different mutant, U43S, whose structure is also reported here, at 1.7 Å resolution. The Sec43Ser mutant of SmGpx (U43S) maintains the same 3D structure of the U43C mutant, thus strongly suggesting that the easier oxidation of Cys43 does not perturb significantly the native structure of the enzyme.

MATERIALS AND METHODS

Mutagenesis and protein expression

The U43C SmGpx gene, with codons optimized for *E. coli* expression (GeneArt AG, Germany), was cloned between BamHI and XhoI restriction sites of a pGex4T-1 expression vector (GE-Healthcare) to obtain a glutathione-S-transferase (GST)-fusion protein. To obtain the second recombinant mutated protein U43S, a mutagenesis experiment was carried out using the QuickChange Site-Directed Mutagenesis Kit (Stratagene). The U43C SmGpx expression vector was used as template and two oligonucleotides containing the mutated serine codon AGC (5′-CGTGGCGTGCAAAAGCGGCGCGACCG-3′; 3′-CGGTCGCGCCGCTTTTGCACGCCACG-5′) were synthesized (Primm srl, MI-Italy) and used as primers.

Both U43C and U43S proteins were expressed in *E. coli* BL21(DE3) cells (Novagen) upon induction with

IPTG 0.5 m*M* overnight at a temperature of 25°C. All reagents were of analytical grade.

Protein purification

Two methods were used for the purification of recombinant U43C SmGpx, so after centrifugation the cells were divided into two stocks. Lysis buffer composed of 20 m*M* Tris/HCl, 0.2M NaCl, 5 m*M* TCEP, 0.1% TrytonX-100, DNase, 1 m*M* PMSF, 1 m*M* EDTA (2-[2-(Bis(carboxymethyl)amino)ethyl-(carboxymethyl)amino]-acetic acid), pH 7.4 was added to one of the two samples before sonication. U43C SmGpx was purified from the soluble fraction through affinity chromatography using a GSH-Sepharose column (GE-Healthcare), and GST was cleaved with bovine thrombin (Sigma). The second protein sample was purified by ionic exchange chromatography. The purification was performed adding 10 m*M* GSH to the lysis buffer to assure the maintenance of a reduced environment both during cell lysis and protein purification. To purify the protein, after sonication, the soluble fraction was applied on a HiTrap SP FF column (GE-Healthcare) equilibrated with the starting buffer 20 m*M* Tris/HCl, 20 m*M* NaCl, 5 m*M* TCEP, 5 m*M* GSH, 1 m*M* EDTA, pH 7.4. U43C protein was eluted by continuous salt gradient using a second buffer with a higher ionic strength (100 m*M* Tris/HCl, 0.5 *M* NaCl, 5 m*M* TCEP, 5 m*M* GSH, 1 m*M* EDTA, pH 7.4). The eluted protein was then cleaved with bovine thrombin. Recombinant U43S protein was purified through GST-affinity chromatography, as described previously for U43C SmGpx.

For each purification the purity of the protein was assessed through overloaded SDS-PAGE, showing a single band corresponding to 19.4 KDa. The purified protein was then dialyzed in 20 m*M* Tris/HCl, 0.1 *M* NaCl, 1 m*M* dithiothreitol (DTT), 0.5 m*M* EDTA, pH 7.4, concentrated by ultrafiltration (Amicon) and stored at −20°C.

SmGpx enzymatic assay

The activity of U43C and U43S SmGpx was assayed in a coupled reaction with Yeast glutathione reductase (GR; Sigma), measuring the decrease of A_{340} as a consequence of the reduction of the hydroperoxide by U43C protein. The assay mixture, composed of 1 μ*M* U43C SmGpx, 0.2 m*M* NADPH, 3 m*M* GSH, 1 unit of GR, in 20 m*M* Tris/HCl, 0.1 *M* NaCl, pH 7.4, was incubated for 5 min at 25°C. The reaction started with the addition of 100 μ*Mtert*-butyl-hydroperoxide or hydrogen peroxide.

Size exclusion chromatography

U43C SmGpx assembly was assayed by gel filtration in HPLC with a Superdex75™ column (GE Healthcare). The protein was concentrated up to 5 mg/mL and a sample volume of 100 μL was applied to the column, which was run at 0.4 mL/min flow. The following buffer was used 20 m*M* Tris/HCl, 0.1 *M* NaCl, 1 m*M* DTT, 0.5 m*M* EDTA, pH 7.4.

Crystallization

A solution of 15 mg/mL U43C or U43S SmGpx was used to screen the crystallization conditions by mean of an automated robotic system (Phenix, Art Robbins). Refinement of the crystallization conditions was done by hand in sitting drop vapor diffusion 24-well plates, with symmetric drops of 1 μL each of protein solution and reservoir.

After 4 days crystals of U43C mutant were obtained in the drops with the following well solution: 0.2 *M* $LiSO_4$, 0.2 *M* Na Acetate, 24% PEG 8000, pH 4.5. A longer time of 7 days was required to obtain good crystals of U43S SmGpx using a well solution of 0.2 *M* NaH_2PO_4, 0.1 *M* MES, 32% PEG-MME 5000, pH 6.0.

Data collection, processing and refinement

X-ray data collection was performed at the synchrotron beamline ID29 at ESRF (Grenoble, France) with an ADSC Q315R detector for U43C SmGpx, while data collections of U43S crystals were performed at the synchrotron beamline ID14.2 at BESSY (Berlin, Germany) with a MARCCD detector. All data were indexed with Mosflm and processed with programs of the CCP4 Suite.[34] U43C mutant crystallized in a $P2_12_12_1$ space group with cell dimension of $a = 41.40$ Å, $b = 60.62$ Å, $c = 62.54$ Å, $\alpha = \beta = \gamma = 90°$, and 1 molecule in the asymmetric unit. The structure was solved by molecular replacement using human HsGpx4 as model (PDB code: 2OBI, 13). U43S mutant showed the same space group but slightly different cell dimensions of $a = 39.91$ Å, $b = 51.17$ Å, $c = 90.62$ Å, $\alpha = \beta = \gamma = 90°$. In this case the structure of U43C SmGpx was used as model for the molecular replacement. Molrep and Refmac programs were used respectively for the molecular replacement and the successive refinements[34]; the structures were built using COOT.[35] Figures were produced with CCP4mg.[36] The quality of the models was assessed with MolProbity[37] and ProCheck.[38] Data collection and refinement statistics are summarized in Table I. The structures were deposited at RCSB Protein Data Bank (U43C SmGpx PDBcode: 2v1m; U43S SmGpx PDBcode: 2wgr).

Sequence alignment

The ClustalW2[39] server was used to obtain a multiple alignment between SmGpx1-2, SjGpx, HsGpx1-4, and BtGpx1 sequences, extracted from NCBI protein sequence database.

Table I
Crystallographic Data Collection and Refinement Statistics

Data collection	U43C SmGpx	U43S SmGpx
Space group	$P2_12_12_1$	$P2_12_12_1$
Cell dimensions		
a, *b*, *c* (Å)	41.40, 60.62, 62.54	39.91, 51.17, 90.62
α, β, γ (°)	90, 90, 90	90, 90, 90
Resolution (Å)	41.38/1.00 (1.05/1.00)[a]	45.31/1.70 (1.79/1.70)[a]
R_{sym} or R_{merge}	0.098 (0.313)[a]	0.077 (0.159)[a]
$I/\sigma I$	17.8 (2.4)[a]	17.3 (9.3)[a]
Completeness (%)	100 (95.32)[a]	99.7 (100)[a]
Redundancy	6.3 (4.9)[a]	5.3 (5.4)[a]
Refinement		
Resolution (Å)	41.38–1.00	90.54–1.70
No. reflections	100,817	112,663
R_{work} / R_{free}	0.17/0.18	0.18/0.21
No. atoms	1616	1482
Protein	1387	1333
Ligand/ion	14	9
Water	215	140
B-*wilson*	4.13	12.7
B-*overall*	6.29	10.6
R.m.s deviations		
Bond lengths (Å)	0.022	0.015
Bond angles (°)	1.958	1.406

[a]Highest resolution shell is shown in parenthesis.

Surface analysis

To look for static cleft and/or cavities to detect GSH and phospholipids binding sites the deposited coordinates were analyzed with the online program CASTp (http://sts-fw.bioengr.uic.edu/castp/index.php), using the server default value of 1.4 Å as probe radius.

Molecular dynamic simulations

The starting coordinates employed for the simulations were taken from the X-ray structure at 1.0 Å resolution of the U43C mutant of *S. mansoni* Gpx, replacing the sulfonic SO_3^- group with the Se^- or SeOH group. Thus, the selenocysteine (Sec) in reduced wild type GPx was modeled as deprotonated, while selenenic derivative (SeOH) in oxidized Gpx was considered as protonated.

In order to determine the partial charges of Sec and its selenenic derivative (SeOH) we performed the quantum chemical calculations on the isolated ethyl selenolate ($CH_3CH_2Se^-$) and methyl selenenic acid (CH_3SeOH), respectively. Density functional calculations, Becke's three parameters exchange,[40] and Lee, Yang, Parr correlation (B3LYP)[41] were performed using the Ahlrichs VTZ basis set.[42] All quantum chemical calculations were carried out using the Gamess US package.[43] Partial charges were obtained from the CHELPG algorithm.[44] The same calculations were performed on analogs, as ethanol or ethanthiol, to test the reliability of the procedure, obtaining partial charges in agreement with the force field used. The following set of partial charges were chosen: for selenolate group of Sec, −0.85 *e* for the Se atom and −0.15 *e* for the C_β atom, while for selenenic group of the Sec derivative, 0.2 *e* for the Se atom, −0.65 *e* for the O atom and 0.45 *e* for the H atom. Nonbonded parameters for selenium were set to $\sigma = 0.458$ nm and $\varepsilon = 1.154$ kJ/mol.[45] The force constants of bonded interactions for selenium were taken to be identical to those for sulfur while the equilibrium values were changed. In particular we set the C—Se bond to 1.95 Å, the Se—O bond to 1.82 Å, the C—C—Se angle to 108°, the C—Se—O angle to 97° and Se—O—H angle to 116°.

Each protein was solvated in a box with explicit SPC water molecules.[46] Three Cl^- for Gpx(Se^-) and four Cl^- for Gpx(SeOH) were added, to provide a neutral simulation box. For all systems, the solvent was relaxed by energy minimization followed by 50 ps of MD at 293 K, while restraining protein atomic positions. The systems were then minimized without restraints and their temperature brought to 293 K in a step-wise manner, before starting the production runs of 30 ns. MD simulations were performed with the Gromacs software package[47] using GROMOS96 force field.[48] Simulations were carried out at constant temperature of 293 K. The Lincs algorithm[49] to constrain bond lengths and the rototranslational constraint algorithm[50] were used. The temperature was held constant by the isothermal algorithm.[51] The Particle Mesh Ewald (PME) method[52] was used for the calculation of the long-range interactions. A time step of 2 fs was used. We used the essential dynamics technique[53] to characterize the dynamical behavior of the protein. The package SURFNET[54] was used for detecting the clefts on the protein surfaces and estimating their volumes. Cavity volumes were evaluated without taking into account the presence of water molecules.

Docking method

Molecular docking was performed using the PatchDock algorithm.[55] Two files of coordinates, for SmGpx (2v1m) and for the phosphatidylcholine (CPL), enriched with hydrogen atoms, were used as input for the program. After setting the RMSD to 9, PatchDock output was a list of potential protein-ligand complexes, among which we choose the solution with the highest geometric shape complementarity score.

RESULTS

Sequence alignment

Sequence alignment of SmGpx with other isoenzymes of all four groups shows higher similarities with the enzymes classified as Group 4 (Fig. 1). Indeed SmGpx presents some residues which are highly conserved in all Gpxs, including the well-known catalytic residues Cys43, Gln78, Trp132, and Asn133. On the other hand, it lacks the conserved residues, apparently involved in GSH bind-

Figure 1

Sequence alignment of SmGpx with Gpx of all classes. Identical residues are highlighted in yellow, conserved residues are boxed. Sm, *Schistosoma mansoni*; Sj, *S. japonicum*; Hs, *Homo sapiens*; Bt, *Bos taurus*.

ing (seemingly Arg57, Arg185, and Met147 in bovine Gpx[10]) and two insertion sequences (i.e., residues 132–154 and 101–104 in HsGpx1), peculiar of the tetrameric Gpxs. These features of the primary structure clearly assign SmGpx to the class of Gpx4. The classification is further confirmed by the conservation of the fold.[56] Indeed superposition of SmGpx with human HsGpx4 [Fig. 2(E)] shows that the main secondary structure motifs are conserved and, consistently, gel-filtration and analytical ultracentrifugation (data not shown) confirmed the monomeric nature of U43C SmGpx. Yet local differences are present, the most obvious being the dislocation of the loop containing residues from 122 to 130 ($\alpha 2-\beta 3$ loop) in U43C mutant and the pocket containing the catalytic residues, together with a few mutations around the active site, including residue 45, a highly conserved Lys in all Gpx4 changed here into Ala, residue 41 (Ser to Cys) and residue 48 (Val to Lys).

Overall structure of U43C and U43S SmGpxs

The crystal structure of U43C SmGpx, solved by molecular replacement using human's HsGpx4 structure as the model (2OBI),[20] confirms that the protein is monomeric. The diffraction data, collected up to 1.0 Å resolution, were refined to the final R_{factor} and R_{free} values of 17.5 and 18.4%, respectively. The validation programs[37,38] showed a very good final geometry and density fit, with all residues lying in the preferred regions of the Ramachandran plot (Table I). The flexibility of the molecule is extremely limited; the high resolution allowed us to place only nine side chains in alternative conformations. Very weak electron density map at the N-terminal region prevented us from placing the first six residues. The average B-factor is 6.29 $Å^2$, with slightly higher values restricted to the ill defined side chains of a few superficial Lys.

U43C SmGpx, like other Gpxs, shows some differences with the typical Trx fold,[57] characterized by 4 β strands flanked by 3 α helices. U43C SmGpx presents a N-terminal extension including two more β strands and an insertion with one more β strand and one α helix. For the sake of consistency, these secondary structure elements are named β1a, β1b, β2a and α1a, as shown in Figure 2(A,B).

The central β sheet of U43C SmGpx contains four β strands: two of them (β3, β4) are antiparallel and connected to the C-term helix α3 to form the typical ββα Trx motif; the other two parallel strands (β1, β2) flank helix α1 to form a βαβ structural motif. Helix α2, perpendicular to α1 and α3, connects β2 and β3 strands through a linking region containing the additional α1a and β2a motifs. Far from the central core and closer to the N-terminal region, the topological diagram shows the last structural motif of U43C SmGpx composed by two antiparallel β strands (β1a, β1b) [Fig. 2(A)].

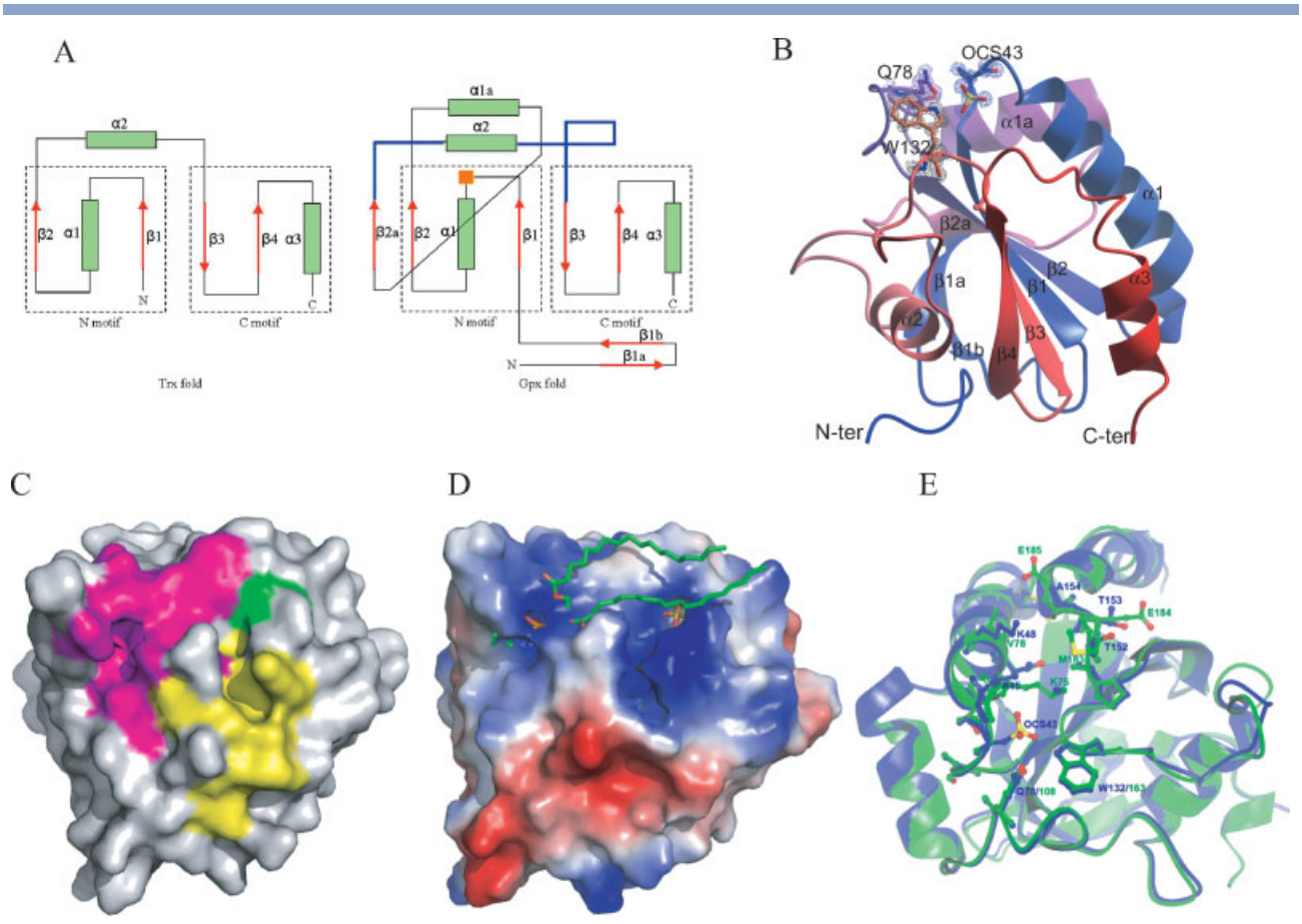

Figure 2

Topological diagrams, overall 3D structure, charge distribution, and dynamic clefts detected on the surface of U43C SmGpx. Panel **A**. Topological diagrams for Trx fold (left) and Gpx fold (right), redrawn from Martin.[50] The blue lines indicate the loops preceding and following helix α2, related to the fluctuations of the putative GSH binding site (see text); the orange box indicates the position of OCS43. Panel **B**. Ribbon representation showing the overall structure of U43C SmGpx. Color blending from N-terminus (blue) to C-terminus (Red). The active site residues, including sulfonated catalytic Cys (OCS43), Gln 78, Trp 132, are shown as ball and stick and contoured with 2Fo-Fc electron density map at 1σ. Panel **C**. Representation of the clefts detected by MD analysis in SmGpx. Yellow: active site cleft; magenta: secondary cleft (putative GSH binding site); green: catalytic Sec residue placed between the two clefts. Panel **D**. Representation of the electrostatic surface potential of U43C SmGpx and docking of phosphatidylcholine (PDB code CPL) on the active site cleft. The phosphorous atom is located in the negative pocket hosting a sulfate anion in the crystal structure, and the two fatty acid chains lie on top of the hydrophobic surface just above OCS43 (same orientation as in Panel C). Panel **E**. Superposition of U43C SmGpx (blue) and HsGpx (green). View of the two proteins from the top looking into the cleft surrounding the catalytic triad; residues different among the two are shown as ball and stick.

The tertiary structure of U43C mutant also contains a few loops, one of which, connecting β1 to α1, hosts the catalytic cysteine (Cys43), which we found oxidized to sulfonic acid (Ocs43) [Fig. 2(B)]; in the structure of human U73C Gpx4 (HsGpx4) this residue is reduced. Yet the geometry of the active site is conserved: in particular the other two residues of the catalytic residues, Gln78 and Trp132, known to be invariant in all Gpx isoforms, are at H-bond distance with Ocs43 [Fig. 2(B)]. This is not surprising given their supposed role in the stabilization of the reduced form of the native enzyme ($R—Se^-$) during catalysis.

To explore the onset of the oxidation of Cys43, we found by MS that the molecular weight of the freshly purified protein is compatible with a reduced Cys residue. We conclude that oxidation of Cys43 should occur during crystallization. In spite of being reduced, the freshly prepared U43C SmGpx is inactive, at least with the substrates tested (*tert*-butyl-hydroperoxide and hydrogen peroxide).

A possible consequence of the oxidation of Cys43 may be a local distortion of the active site structure, that should accommodate the bulky sulfonic acid. This possibility seems unlikely, given that the structure of U43C SmGpx is similar to that of other class 4 Gpxs. However, to demonstrate this point, we prepared and structurally characterized the U43S mutant.

The crystal structure of U43S mutant was solved by molecular replacement using the U43C SmGpx structure

as the model (2v1m). Data were collected up to 1.7 Å resolution and refined to the final R_{factor} and R_{free} values of 18.2 and 21.2%, respectively. The validation programs[37,38] showed a very good final geometry and density fit, with all residues lying in the preferred regions of the Ramachandran plot. Data collection and refinement statistics are shown in Table I.

Quantitative comparison of U43S with U43C SmGpx did not show any significant structural difference neither in the stereochemistry of the residues into the active site nor in the 3D structure of the protein at large ($RMSD_{main\ chain}$=0.38 Å; $RMSD_{side\ chain}$=1.21 Å).

Surface analysis

In superposing U43C/U43S SmGpx with human HsGpx4, some differences appear. The active site pocket of U43C SmGpx is exposed to the solvent and has a strong positive surface charge, which may favor the binding of negatively charged ligands near Sec43 [Fig. 2(D)]. On the other hand in HsGpx4 the pocket is less exposed to the solvent, less positive and more hydrophobic, shielding the mutated active site C73.

The electrostatic surface of the protein displays an overall positive charge [Fig. 2(D)] which is significantly more extended in U43C/U43S SmGpx than in HsGpx4. In particular, many basic amino acids form a superficial positive channel, a sort of rim around the residue at position 43. Opposite to this channel we can identify one of the few negatively charged regions of the protein surface, due to the high local concentration of acidic residues. The human enzyme, instead, displays a more pronounced overall negative and hydrophobic surface, the latter around the active site, in particular.

From the electrostatic surface representation, the catalytic site of HsGpx4 seems partially hindered (as indicated by CASTp analysis). We have identified two topologically equivalent cavities in U43C SmGpx and human HsGpx4, which however have different areas and volumes (140Å^2/94Å^3 for U43C SmGpx and 93Å^2/72Å^3 for HsGpx4, respectively). Superposition of the two structures with SSM methods shows a few point mutations involving the residues surrounding the pocket: A45, K48, T153, and A154 in SmGpx are respectively mutated in Lys, Val, Glu, and Glu in the human enzyme. A contribution to the greater extension of SmGpx pocket may be attributed to the lack of the H-bond between Glu158 and Gln52, which in the human enzyme partially closes the pocket, and shields the catalytic Cys73 from direct access to the solvent [Fig. 2(E)].

Static and dynamic analyses of U43C SmGpx show the existence of a solvent exposed cleft, containing the active site residues. This cleft, as determined by CASTp analysis, is divided in two halves by a ridge that hosts C43 (Ocs43), whose volume is increased because of oxidation, and which seems to act as a flexible barrier in between.

Table II
The Amino Acid Residues Lining the Clefts Identified by the Static and Dynamic Analysis of SmGpx

	CASTp on U43C crystal structure	MD simulation on SmGpx
Residues in the active site cleft	OCS43	Sec43
	Ala45	
	Lys48	**Lys48**
	Asn49	**Asn49**
	Gln52	**Gln52**
	Trp132	**Trp132**
		Phe134
	Lys 136	**Lys136**
	Pro151	
	Thr152	**Thr152**
	Thr153	**Thr153**
	Ala154	**Ala154**
	Pro155	**Pro155**
		Tyr156
		Glu159
		Ile162
Residues in the secondary cleft (putative GSH binding site)		Gly124
		Thr125
		Asn129
	Ile130	**Ile130**
	Lys131	**Lys131**
	Trp132	**Trp132**
	Ser135	**Ser135**
	Arg148	**Arg148**
		Tyr149
		Ser150
		Pro151

The active site cleft is delimited by Hydrophobic, polar and aromatic Residues; the secondary cleft (Smaller than the active site One) has a Greater density of positive Charges. Residue detected in Both static and dynamic analysis are shown in bold.

Elimination of sulfonic acid by mutation of Cys43 to Ser or by computational methods, does not change significantly this condition, except that the physical barrier between the two half-clefts is less prominent. On one side of the ridge, we identified a putative active site cleft with better access to C43 (yellow surface in Fig. 2C), which has surface area and volume of about 140Å^2 and 94Å^3, respectively, and is delimited by hydrophobic, polar and aromatic residues (Table II). On the opposite side of C43, CASTp identifies a secondary crevice, with limited access to C43, centered around Lys131 and having area and volume of about 107Å^2 and 57Å^3, respectively. Although the latter is smaller than the active site one, the density of positive charges is greater.

Unfortunately we could not obtain a structure with GSH/GSSG bound. Previous functional and structural studies on other Gpx did not provide direct evidence about the stereochemistry of GSH in the catalytic pocket. However Epp et al.[10] proposed a model based on differences in the electron density maps between the oxidized and GSH reduced wild type bovine cellular enzyme (1GP1). They concluded that three residues (Arg57, Arg184, and Met147) are involved in GSH binding. Sequence alignment and structural superposition allowed

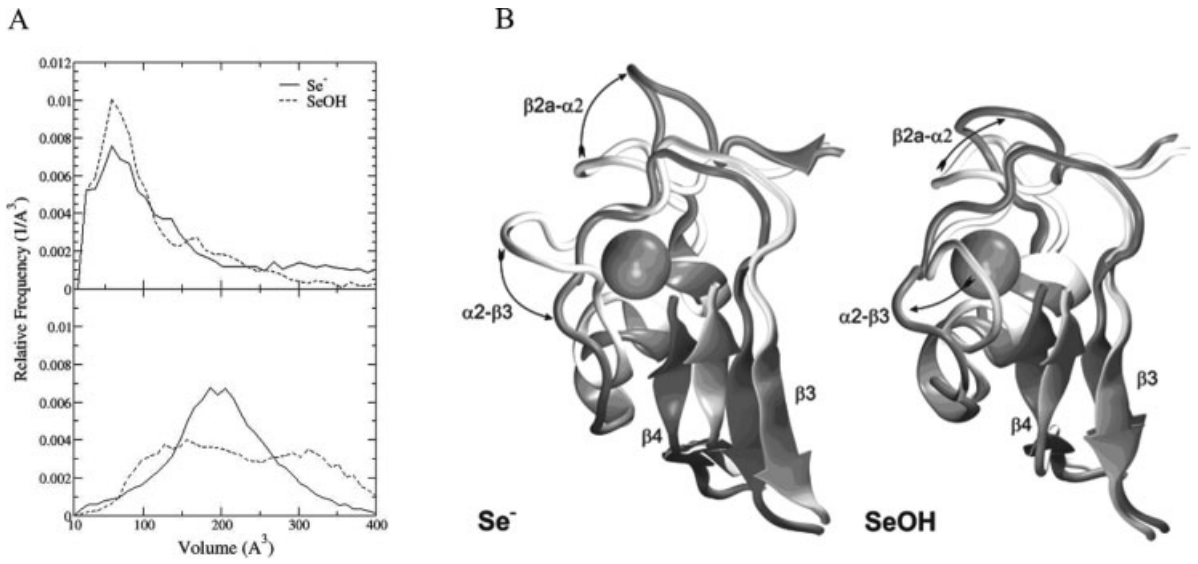

Figure 3

Active site and secondary half cleft identified by MD simulations. Panel **A**. Relative frequency of the volume distributions of the active site cleft (upper panel) and of the secondary positively charged cleft (bottom panel), shown for the reduced (Se^-, solid lines) and the oxidized (SeOH, dashed lines) states of SmGpx. Panel **B**. Extreme configurations from the most different eigenvalues for each simulation of reduced (Se^-) and oxidized (SeOH) SmGpx. The directions of motion of the loops (β2a–α2, α2–β3) preceding and following helix α2 are shown. The approximate position of the secondary half cleft limited by the two loops is highlighted by a sphere.

us to trace the equivalent positions in U43C SmGpx. This putative GSH binding site overlaps with our secondary cleft, even though the residues that should interact with GSH are quite different. While the putative role of Arg57 could be played in U43C SmGpx by Lys48, Arg184 is mutated to Pro150 and an equivalent of Met147 is absent, being localized in a loop of residues involved in the dimerization of oligomeric Gpxs. In view of these differences, the hypothesis that the functional role of our secondary cleft is to provide the actual GSH binding site must be considered with caution; moreover, the dynamic volume fluctuations of this cleft and the absence of independent information prevented our attempts to model the binding of GSH or GSSG.

Molecular dynamics simulations:

The experimentally determined 3D structure of U43C SmGpx poses two questions pertinent to the catalytic activity of the enzyme, namely: (i) whether the oxidation of Cys43 to sulfonic acid perturbs the overall structure of the protein; and (ii) what is the topology and geometry of both the active site and the secondary, putative GSH binding, cleft. These questions were addressed by MD simulations.

1) No differences were detected in a comparison between the crystallographic structure of U43C and that of wild type SmGpx in both the reduced and oxidized states, as obtained from MD simulations. Hence the *in silico* replacement of the SO_3^- group with functional Se^- or SeOH groups, not only did not significantly perturb the structure, as shown by agreement between the experimental and computational results, but also permitted to study the structural and the dynamical behavior of the two oxidation states of wtSmGpx, presumably populated during the catalytic cycle.
2) During the simulations, transiently formed cavities with volumes ranging from 10 to a few hundreds $Å^3$ are detected on the surface, close to residue 43, with an occurrence of 15–20% of simulation time. These cavities are coupled to the active site cleft as detected by CASTp (Table II) and, when they are open, they increase the volume of the active site. The volume distributions of such cavities, reported in Figure 3(A) for reduced and oxidized SmGpx (volume >10 $Å^3$), are by-and-large independent of the oxidation state of Sec.

The reason for exploring both redox states is due to the fact that the suggested mechanism for the reaction catalyzed by Gpxs is a ping-pong one, with the Se atom of Sec shuttling between two redox states: selenolate anion ($R—Se^-$) and selenenic acid (R—Se—OH). Upon reduction of hydroperoxides, the selenolate anion is oxidized to selenenic acid, which in turn is reduced by GSH.[57]

During MD simulations a secondary positively charged cleft close to Lys131 is detected for a fraction of time of

80–85% for both reduced and oxidized SmGpx [Fig. 3(A)]. In reduced SmGpx the volume distribution is characterized by a large single peak with a maximum at about 200 $Å^3$, while in oxidized SmGpx it is significantly broader and almost flat, with values ranging from 100 to 300 $Å^3$. The core of this cleft has been also detected by CASTp in the static structure of U43C SmGpx with a volume of ~57 $Å^3$. Therefore, MD suggests that both clefts detected by CASTp undergo transient expansion that may be functionally relevant, since their volume from the static crystal structure appears too small to accommodate either substrate (i.e., the organic hydroperoxides or GSH).

Although the loops preceding and following helix α2 only to a minimal extent participate to the secondary cleft, their motions are specifically correlated to the fluctuations of the putative GSH binding site, as detected by essential dynamics (ED) analysis,[53] performed on the backbone of amino acids 104 to 140. The eigenvectors with larger eigenvalues correspond to the principal directions of motion of these residues, which form the β3 strand, the helix α2 and two loops, i.e., the β2a–α2 loop (residues 104–112), and the α2–β3 loop (residues 122–134), which is closer to the positive cleft. In Figure 3(B) we report the extreme configurations corresponding to the opposite values of the projection on the first eigenvector as determined from the simulations of SmGpx(Se^-) and SmGpx(SeOH), respectively. The approximate position of the cavity is highlighted by a sphere. It is interesting to note that the principal motions of the two loops, β2a–α2 and α2–β3, are correlated in both oxidation states. Clearly, in SmGpx(SeOH) the displacement of the β2a–α2 loop toward the active site is coupled with a displacement of the α2–β3 loop away from the β4 strand and thereby an increase of the cleft volume. On the other hand, in SmGpx(Se^-) the coupling between the two loops is anticorrelated, since, when the β2a–α2 loop moves toward the active site, the distance between the α2–β3 loop and the β4 strand decreases and the cleft volume shrinks.

Finally the mean density distribution of chloride ions around the protein surface confirms that native SmGpx, both in the reduced (Se^-) and oxidized (SeOH) states, is characterized by a bipolar charge distribution. In particular the surface portion, rich in basic residues and delimited by K105, K116, K119, and K131, is characterized by a strong positive electrostatic potential, while on the side of the protein corresponding to the N-terminal βαβ motif negative potential is predominant.

DISCUSSION

The mutant SmGpxs U43C and U43S proved to be inactive at every stage of purification, starting from the cell lysate; this was expected in the case of U43S and unexpected in that of U43C. We used different purification protocols (see Methods) employing several reducing agents, including TCEP, DTT, β-Mercaptoethanol, GSH; unfortunately all attempts were unsuccessful. The crystal structure revealed the oxidation of Cys43 to sulfonic acid (OCS), but this is unlikely to be the (only) cause for the absence of activity, given that oxidation occurs (mainly) during crystallization, as demonstrated by mass spectrometry. We attempted to provide an interpretation by comparing U43C SmGpx with U73C of HsGpx4, with human Gpx1, and with bovine Gpx. Superposition of 3D structures shows that two of the three oxygen atoms bound to the oxidized Cys43 of SmGpx are located in the same positions as the oxygen atoms of the selenenic acid present in human Gpx1 or bovine Gpx. Although the oxidized state of Cys43 to sulfonic acid is artificial, one may speculate that it resembles the oxidized selenol group populated during the catalytic cycle. This hypothesis is supported by the observation that the mutation Sec/Cys, Sec/Ser and the oxidation of Cys do not cause any relevant structural rearrangement of the catalytic pocket, as also confirmed by MD. The additional characterization of U43S SmGpx, which did not show any real deviation from the U43C structure, further supports this fact making it reliable that the structures solved are consistent with the native structure of SmGpx, especially concerning the catalytic site of the enzyme.

An important question raised by the U43C structure is why Cys43 is so prone to auto-oxidation, in view of the fact that this reaction is not usually observed in other Sec to Cys mutated Gpxs. We haven't come to a conclusion about the molecular basis for promotion of Cys oxidation and its possible *in vivo* relevance. The active site of SmGpx is indeed more reactive than that of other Gpxs, as supported by the fact that analogous mutants are not oxidized. In Table III, we have listed the contacts of the active Cys in U43C SmGpx and HsGpx4. The most obvious differences lie in the greater polarity of U43C SmGpx active site, favoring access to water and possibly metal ions that could exert a catalytic role. Aside from this and from the different volume of the pocket around OCS43, a specific role for surrounding residues is not immediately apparent. Nevertheless the charge distribution around the catalytic residue might be changed by the following substitutions: Cys41 of U43C SmGpx to Ser in HsGpx4 and Ala45 to Lys.

It is known from functional studies that class 4 Gpx prefer phospholipid hydroperoxides as substrates over-and-above H_2O_2 or other organic hydroperoxides.[59] Moreover, it is known that schistosome, being unable to synthesize *de novo* fatty acids, uploads them from the host and adult worms usually use oleate (18:1) from the host and elongate the chain to eicosenoate (20:1), which is incorporated predominantly in the phosphatidylcholine molecule together with palmitate (16:0).[60] Thus, we have attempted to identify in U43C SmGpx a possible binding site for phosphatidylcholine (PC) in the proximity of

Table III
Inter Residue Contacts Around the Active Ocs43/Cys73 in U43C and Human HsGpx4 Respectively. Distances Shown are Between Each Residue and the Catalytic Ocs43/Cys73. Putative H-bonds (in bold) have been Identified Choosing a Bond Length Cut-Off of 3.10 Å[64] and Allowing for an Experimental Error of 0.05 Å; Moreover, Their Bond Angles have been Checked and demonstrated to be Compatible with the Expected Linear Geometry[a]

SmGpx			HsGpx4		
Atom 1	Atom 2	Distance	Atom 1	Atom 2	Distance
43OCS/O	45 ALA/N	3.11	73CYS/O	75 LYS/N	3.12
	46 THR/OG1	3.03		76 THR/OG1	3.03
	46 THR/N	**3.04**		**76 THR/N**	**3.01**
	61 HOH	**3.12**			
43OCS/N	41 CYS/O	3.78	73CYS/N	71 SER/O	3.79
	46 THR/OG1	**3.03**		**76 THR/OG1**	**3.12**
43OCS/SG	44 GLY/N	3.39	73CYS/SG	75 LYS/N	3.48
	132 TRP/NE1	3.84		181 TRP/NE1	3.92
	74 HOH	3.75		164 ASN/ND2	3.63
43OCS/OD1	78 GLN/NE2	3.86			
	132 TRP/NE1	3.49			
	44 GLY/N	3.11			
43OCS/OD2	132 TRP/NE1	3.08			
	133 ASN/ND2	**2.91**			
	74 HOH	**3.09**			
43OCS/OD3	44 GLY/N	3.22			
	45 ALA/N	**2.79**			
	46 THR/N	3.89			
	74 HOH	3.27			

[a]To describe how the angles were determined, we schematically represent the H-bond as X—D—H···A, where D is the donor atom and A is the acceptor. In our maps the H atom is not detected, thus the linear arrangement of atoms D—H···A cannot be checked directly. However, linearity can be safely assumed if the D—A distance is below the threshold and X—D—A angle is compatible with the known hybridization of D.

C43, through docking[55] (Fig. 2D). In spite of the high flexibility of the substrate PC, under the assumption that the phosphate (P) of PC occupies the same site of the sulfate or pyrophosphate anion present in U43C SmGpx and U43S SmGpx, respectively, we identified a plausible binding site comprising: (i) the residues surrounding the active site cysteine (43–45 and 74–77) (the Cys residue should act on the peroxidatic double bond of the phosphatidylcholine hydroperoxide fatty acid chains) and (ii) those surrounding the strongly positive pocket (57 $Å^3$) next to the catalytic Cys hosting a sulfate/pyrophosphate anion (residues 123–133 and 148–151). In fact MD simulations have shown that such a pocket undergoes relevant expansions in solution, enabling it to accommodate larger substrates; moreover, pocket volume fluctuations seem to be regulated by the redox state of the protein, making a sort of ping–pong mechanism plausible.[61] The program Patchdock optimized the position of the substrate, with the following constraint: P to R148 distance = 3.9 Å. Although this procedure is somewhat arbitrary, it is useful to suggest a possible orientation of a highly flexible substrate. It seems that when the phosphate group of the phosphatidylcholine is located in the pocket containing the sulfate or pyrophosphate anion, the two fatty acid hydrophobic chains may lodge on top of a large hydrophobic surface located above the catalytic cysteine, positioning C43 close to C_9–C_{10} double bond of the eicosenoic acid. This observation may have a functional relevance as it is known that over-oxidation of unsaturated fatty acids occurs usually on a double bond located around C10 yielding similar oxidation products for monoene-, diene-, and triene-fatty acids.[62]

The substrate specificity of class 4 Gpx for phospholipids, besides being proven by functional assays, is also consistent with data obtained by immunolocalization studies, which showed that SmGpx is associated with the tegument and gut epithelium of adult worms,[63] the host-parasite interface. This particular tissue distribution of SmGpx in the worms has made it a candidate of choice for the design of a vaccine against schistosomiasis,[58] like other schistosome antioxidant enzymes (SmSOD and SmGST). Hence, the availability of an atomic resolution structure of this enzyme, though in an inactive state, is a useful first step toward the localization of its epitopes.

ACKNOWLEDGMENT

The authors gratefully acknowledge ESRF for access to synchrotron facilities.

REFERENCES

1. Margis R, Dunand C, Teixeira FK, Margis-Pinheiro M. Glutathione peroxidase family—an evolutionary overview. FEBS J 2008;275: 3959–3970.

2. Arthur JR. The glutathione peroxidases. Cell Mol Life Sci 2000;57: 1825–1835.
3. Herbette S, Roeckel-Drevet P, Drevet JR. Seleno-independent glutathione peroxidase. More than simple antioxidant scavengers. FEBS J 2007;274:2163–2180.
4. Papp LV, Lu J, Khanna KK. From selenium to selenoproteins: synthesis, identity, and their role in human health. Antioxid Redox Signal 2007;9:775–806.
5. Squires JE, Berry MJ. Eukaryotic selenoprotein synthesis: mechanistic insight incorporating new factors and new functions for old factors. IUBMB Life 2008;60:232–235.
6. Zuberbuehler CA, Messikommer RE, Arnold MM, Forrer RS, Wenk C. Effect of selenium depletion and selenium repletion by choice feeding on selenium status of young and old laying hens. Physiol Behav 2006;87:430–440.
7. Maiorino M, Aumann KD, Brigelius-Flohé R, Doria D, Van Den Heuvel J, Mccarthy J, Roveri A, Ursini F, Flohé L. Probing the presumed catalytic triad of a selenium-containing peroxidase by mutational analysis. Z Ernahrungswiss 1998;37:118–121.
8. Holben DH, Smith AM. The diverse role of selenium within selenoproteins: a review. J Am Diet Assoc 1999;99:836–843.
9. Su D, Novoselov SV, Sun Qi-An, Moustafa ME, Zhou Y, Oko R, Hatfield DL, Gladyshev VN. Mammalian selenoproteins thioredoxin-glutathione reductase. J Biol Chem 2005;280:26491–26498.
10. Epp O, Ladenstein R, Wendel A. The refined structure of the selenoenzyme glutathione peroxidase at 0.2-nm resolution. Eur J Biochem 1983;133:51–69.
11. Chu FF, Doroshow JH, Esworthy RS. Expression, characterization and tissue distribution of a new cellular selenium-dependent glutathione peroxidase, GSHPx-GI. J Biol Chem 1993;268:2571–2576.
12. Ren B, Huang W, Akesson B, Ladenstein R. The crystal structure of seleno-glutathione peroxidase from human plasma at 2.9 A resolution. J Mol Biol 1997;268:869–885.
13. Maiorino M, Roche C, Kiess M, Gawlik D, Matthes M, Naldini E, Pierce R, Flohè L. A selenium containing phospholipid-hydroperoxide glutathione peroxidase in *Schistosoma mansoni*. Eur J Biochem 1996;238:838–844.
14. Tosatto SC, Bosello V, Federico F, Mauri P, Roveri A, Toppo S, Flohé L, Ursini F, Maiorino M. The catalytic site of glutathione peroxidase. Antiox Redox Signal 2008;10:1515–1525.
15. Wang Z, Wang F, Duan R, Liu JY. Purification and physicochemical characterization of a recombinant phospholipid hydroperoxide glutathione peroxidase from *Oriza sativa*. J Biochem Mol Biol 2007;40: 412–418.
16. Conrad M, Schneider M, Seiler A, Bornkamm GW. Physiological role of phospholipid hydroperoxide glutathione peroxidase in mammals. Biol Chem 2007;388:1019–1025.
17. Nomura K, Imai H, Koumura T, Arai M, Nakagawa Y. Mitochondrial phospholipid hydroperoxide glutathione peroxidase suppresses apoptosis mediated by a mitochondrial death pathway. J Biol Chem 1999;274:29294–29302.
18. Ursini F, Heim S, Kiess M, Maiorino M, Roveri A, Wissing J, Flohè L. Dual function of the selenoprotein PhGpx during sperm maturation. Science 1999;285:1393–1396.
19. Schnurr K, Belkner J, Ursini F, Schewe T, Kühn H. The selenoenzyme phospholipid hydroperoxide glutathione peroxidase controls the activity of the 15-lipoxygenase with complex substrates and preserves the specificity of the oxygenation products. J Biol Chem 1996;271:4653–4658.
20. Scheerer P, Borchert A, Krauss N, Wessner H, Gerth C, Höhne W, Kuhn H. Structural basis for catalytic activity and enzyme polymerization of phospholipid hydroperoxide glutathione peroxidase-4 (GPx4). Biochemistry 2007;46:9041–9049.
21. Johansson C, Kavanagh KL, Rojkova A, Gileadi O, Von Delft F, Arrowsmith C, Weigelt J, Sundstrom M, Edwards A, Oppermann U. Structural genomics consortium (SGC). Crystal structure of the selenocysteine to glycine mutant of human glutathione peroxidase 4(GPX4) in press.
22. Savioli L, Renganathan E, Montresor A, Davis A, Behbehani K. Control of schistosomiasis—a global picture. Parasitol Today 1997;13:444–448.
23. Angelucci F, Basso A, Bellelli A, Brunori M, Pica Mattoccia L, Valle C. The antischistosomal drug praziquantel is an adenosine antagonist. Parasitology 2007;134:1215–1221.
24. Zelck UE, Janowsky B. Antioxidant enzymes in intramolluscan *Schistosoma mansoni* and ROS-induced changes in expression. Parasitology 2004;128:493–501.
25. Salinas G, Selkirk ME, Chalar C, Maizels RM, Fernàndez C. Linked thioredoxin-glutathione systems in platyhelminths. Trends Parasitol 2004;20:340–346.
26. Angelucci F, Miele AE, Boumis G, Dimastrogiovanni D, Brunori M, Bellelli A. Glutathione reductase and thioredoxin reductase at the crossroad: the structure of *Schistosoma mansoni* thioredoxin glutathione reductase. Proteins 2008;72:936–945.
27. Jaeger T, Flohé L. The thiol-based redox networks of pathogens: unexploited targets in the search for new drugs. Biofactors 2006;27:109–120.
28. Sayed AA, Cook SK, Williams DL. Redox balance mechanism in *Schistosoma mansoni* rely on peroxiredoxins and albumin and implicate peroxiredoxins as novel drug targets. J Biol Chem 2006; 281:17001–17010.
29. Roche C, Williams DL, Khalife J, Lepresle T, Capron A, Pierce RJ. Cloning and characterization of the gene encoding *Schistosoma mansoni* glutathione peroxidase. Gene 1994;138:149–152.
30. Williams DL, Pierce RJ, Cookson E, Capron A. Molecular cloning and sequencing of glutathione peroxidase from *Schistosoma mansoni*. Mol Biochem Parasitol 1992;52:127–130.
31. Mei H, Loverde PT. *Schistosoma mansoni*: cloning the gene encoding glutathione peroxidase. Exp Parasitol 1995;80:319–322.
32. Mei H, Thakur A, Schwartz J, Lo Verde PT. Expression and characterization of glutathione peroxidase activity in the human blood fluke *Schistosoma mansoni*. Infect Immun 1996;64:4299–4306.
33. Salisbury FR, Knutson ST, Poole LB, Fetrow JS. Functional site profiling and electrostatic analysis of cysteines modifiable to cysteine sulfenic acid protein. Protein Sci 2008;17:299–312.
34. Collaborative Computational Project, Number 4. The CCP4 Suite: programs for protein crystallography. Acta Crystallogr Sect D 1994;57:1373–1382.
35. Emsley P, Cowtan K. Coot: model-building tools for molecular graphics. Acta Crystallogr Sect D 2004;60:2126–2132.
36. Potterton L, Mcnicholas S, Krissinel E, Gruber J, Cowtan K, Emsley P, Murshudov GN, Cohen S, Perrakis A, Noble M. Development in the CCP4 molecular-graphics project. Acta Crystallogr Sect D 2004; 60:2288–2294.
37. Davis IW, Leaver-Fay A, Chen VB, Block JN, Kapral GJ, Wang X, Murray LW, Arendall WB, Snoeyink J, Richardson JS, Richardson DC. MolProbity: all-atom contacts and structure validation for proteins and nucleic acids. Nucleic Acids Res 2007;35:W375–W383.
38. Laskowski RA, Macarthur MW, Moss DS, Thornton JM. Procheck—a program to check the stereochemical quality of protein structures. J Appl Crystallogr 1993;26:283–291.
39. Larkin MA, Blackshields G, Brown NP, Chenna R, Mcgettigan PA, Mcwilliam H, Valentin F, Wallace IM, Wilm A, Lopez R, Thompson JD, Gibson TJ, Higgins DG. Clustal W and Clustal X version 2.0. Bioinformatics 2007;23:2947–2948.
40. Becke AD. Density-functional thermochemistry. III. The role of exact exchange. J Chem Phys 1993;98:5648–5652.
41. Lee C, Yang W, Parr RG. Development of the Colle-Salvetti correlation-energy formula into a functional of the electron density. Phys Rev B: Condens Matter 1988;37:785–789.

42. Schaefer A, Horn H, Ahlrichs R. Fully optimized contracted Gaussian basis sets for atoms lithium to krypton. J Chem Phys 1992;97: 2571–2577.
43. Schmidt MW, Baldridge KK, Boatz JA, Elbert ST, Gordon MS, Jensen JH, Koseki S, Matsunaga N, Nguyen KA, Su S, Windus TL, Dupuis M, Montgomery JA, Jr. General atomic and molecular electronic structure system. J Comput Chem 1993;14:1347–1363.
44. Breneman CM, Wiberg KB. Determining atom-centered monopoles from molecular electrostatic potentials. The need for high sampling density in formamide conformational analysis. J Comput Chem 1990;11:361–373.
45. Allinger NL, Allinger JA, Yan LQ. Molecular mechanics (MM2) calculations on organo selenium and tellurium compounds. J Mol Struct 1989;201:363–369.
46. Berendsen HJC, Postma JPM, Van Gunsteren WF, Hermans J. Interaction models for water in relation to protein hydration. In: Pullman B, editor. Intermolecular forces. Dordrecht, The Netherlands: D Reidel Publishing Company; 1981. pp 331–342.
47. Berendsen HJC, Van Der Spoel D, Van Drunen R. GROMACS: a message-passing parallel molecular dynamics implementation. Comput Phys Commun 1995;91:43–56.
48. Van Gunsteren WF, Billeter S, Eising A, Hunenberger P, Kruger P, Mark AE, Scott WRP, Tironi IG. Biomolecular simulations: the GROMOS96 manual and user guide. Zurich, Groningen: BIOMOS b.v; 1996.
49. Hess B, Bekker H, Berendsen HJC, Fraaije JGEM. LINCS: a linear constraint solver for molecular simulations. J Comput Chem 1997; 18:1463–1472.
50. Amadei A, Chillemi G, Ceruso MA, Grottesi A, Di Nola A. Molecular dynamics simulations with constrained roto-translational motions: theoretical basis and statistical mechanical consistency. J Chem Phys 2000;112:9–23.
51. Evans DJ, Morriss GP. Statistical mechanics of nonequilibrium liquids. London: Academic Press; 1990.
52. Essmann U, Perera L, Berkowitz ML, Darden T, Lee H, Pedersen LG. A smooth particle mesh Ewald method. J Chem Phys 1995;103: 8577–8593.
53. Amadei A, Linssen AB, Berendsen HJ. Essential dynamics of proteins. Proteins 1993;17:412–425.
54. Laskowski RA. SURFNET: a program for visualizing molecular surfaces, cavities, and intermolecular interactions. J Mol Graph 1995;13:323–330.
55. Schneidman-Duhovny D, Inbar Y, Nussinov R, Wolfson HJ. PatchDock and SymmDock: servers for rigid and symmetric docking. Nucleic Acids Res 2005;33:W363–W367.
56. Toppo S, Vanin S, Bosello V, Tosatto SCE. Evolutionary and structural insights into the multifaceted glutathione peroxidase (Gpx) superfamily. Antioxid Redox Signal 2008;10:1515–1526.
57. Martin JL. Thioredoxin: a fold for all reasons. Structure 1995; 3:245–250.
58. Lo Verde PT, Carvalho-Queiroz C, Cook R. Vaccination with antioxidant enzymes confers protective immunity against challenge infection with *Schistosoma mansoni*. Mem Inst Oswaldo Cruz 2004; 99:37–43.
59. Thomas JP, Maiorino M, Ursini F, Girotti AW. Protective action of PhGPX against membrane-damaging lipid peroxidation. In situ reduction of phospholipid and cholesterol hydroperoxides. J Biol Chem 1990;265:454–461.
60. Brouwers J, Smeeck I, Van Golde L, Tielens A. The incorporation, modification and turnover of fatty acids in adult *Schistosoma mansoni*. Mol Biochem Parasitol 1997;88:175–185.
61. Prabhakar R, Vreven T, Morokuma K, Musaev DG. Elucidation of the mechanism of selenoprotein glutathione peroxidase (GPx)-catalyzed hydrogen peroxide reduction by two glutathione molecules: a density functional study. Biochemistry 2005;44: 11864–11871.
62. Porter NA, Caldwell SE, Mills KA. Mechanisms of free radical oxidation of unsaturated lipids. Lipids 1995;30:277–290.
63. Mei H, Lo Verde P. *Schistosoma mansoni:* the developmental regulation and immunolocalization of antioxidant enzymes. Exp Parasitol 1997;86:69–78.
64. Khan A. A liquid water model: density variation from supercooled to superheated states, prediction of H-bonds, and temperature limits. J Phys Chem 2000;104:11268–11274.